AGU PUBLICATIONS

Geophysical Research Letters

RESEARCH LETTER
10.1002/2016GL068179

Photoelectron-induced waves: A likely source of 150 km radar echoes and enhanced electron modes

Meers M. Oppenheim[1] and Yakov S. Dimant[1]

[1]Center for Space Physics, Boston University, Boston, Massachusetts, USA

Key Points:
- Origin of 150 km echoes
- Simulations of photoelectron-induced irregularities in the ionosphere
- Answers a long-standing mystery about a geophysical observation

Supporting Information:
- Supporting Information S1
- Movie S1

Correspondence to:
M. M. Oppenheim,
meerso@bu.edu

Citation:
Oppenheim, M. M., and Y. S. Dimant (2016), Photoelectron-induced waves: A likely source of 150 km radar echoes and enhanced electron modes, *Geophys. Res. Lett.*, *43*, 3637–3644, doi:10.1002/2016GL068179.

Received 8 FEB 2016
Accepted 29 MAR 2016
Published online 27 APR 2016

Abstract VHF radars near the geomagnetic equator receive coherent reflections from plasma density irregularities between 130 and 160 km in altitude during the daytime. Though researchers first discovered these 150 km echoes over 50 years ago and use them to monitor vertical plasma drifts, the underlying mechanism that creates them remains a mystery. This paper uses large-scale kinetic simulations to show that photoelectrons can drive electron waves, which then enhance ion density irregularities that radars could observe as 150 km echoes. This model explains why 150 km echoes exist only during the day and why they appear at their lowest altitudes near noon. It predicts the spectral structure observed by Chau (2004) and suggests observations that can further evaluate this mechanism. It also shows the types and strength of electron modes that photoelectron-wave interactions generate in a magnetized plasma.

1. Introduction

Shortly after the large VHF radar at the Jicamarca Radio Observatory (JRO) was deployed in 1962, it detected unexpected echoes at around 150 km altitude [*Balsley*, 1964]. Figure 1 shows two modern examples of these "150 km echoes." Despite decades of investigation, the origin of these reflections remains a mystery. This paper introduces a novel model to explain many aspects of these echoes and presents a series of simulations to show its plausibility.

This paper proposes that 150 km echoes originate due to a multistep process that exists at around 150 km altitude. At these altitudes, UV photons ionize the O_2 or N_2 molecules, creating electrons with energies greatly exceeding the ambient plasma thermal energy of $\sim$ 0.03 eV. These photoelectrons will form a bump-on-tail population, but since the distribution is isotropic in 3-D, the bump takes the form of a phase space shell. In an unmagnetized plasma, such a shell should not produce an instability, but the magnetic field breaks the symmetry of the system and leads to energetic particle-driven wave growth. In particular, the shell interacts with the background electrons to generate upper hybrid, electron Bernstein, and Langmuir waves. These electron waves then couple to oblique ion-acoustic waves, perpendicular $\omega = 0$ modes, and lower hybrid modes, generating irregularities that radars detect as 150 km echoes.

This model explains many features of 150 km echoes. It easily explains why they exist only in daylight. It explains the necklace shape because EUV photons penetrate most deeply at noon and less so at other times of the day as the photons have to travel through more atmosphere before encountering the same depth. It also explains why the echoes disappeared during the partial solar eclipse observed over the Gadanki radar site [*Patra et al.*, 2011] and why they were enhanced during a solar flare [*Reyes*, 2012]. It may explain why they show the vertical structuring seen in Figure 1 by invoking resonances which optimize this process at some altitudes and not others. It further explains why the most intense 150 km echoes have a narrow spectral width and are strongly field aligned while they also produce less strongly field-aligned waves with far broader spectral widths [*Chau*, 2004]. This model does not explain why the waves do not appear at higher latitudes. One can speculate that the rapidly changing conductivity along geomagnetic field lines shorts out the process. Also, a lack of highly sensitive radars capable of measuring field-aligned waves at these latitudes may preclude our ability to observe these low-amplitude waves.

1.1. Background

A number of large radars observe 150 km echoes or plasma modes, though none currently does both simultaneously. The most thorough observations of 150 km echoes come from the 50 MHz radar at JRO *Chau and Kudeki* [2013]. However, these echoes have also been observed at other equatorial sites with radars having different characteristics [*Patra et al.*, 2011; *Rodrigues et al.*, 2013; *Yokoyama et al.*, 2009]. The Arecibo Radar

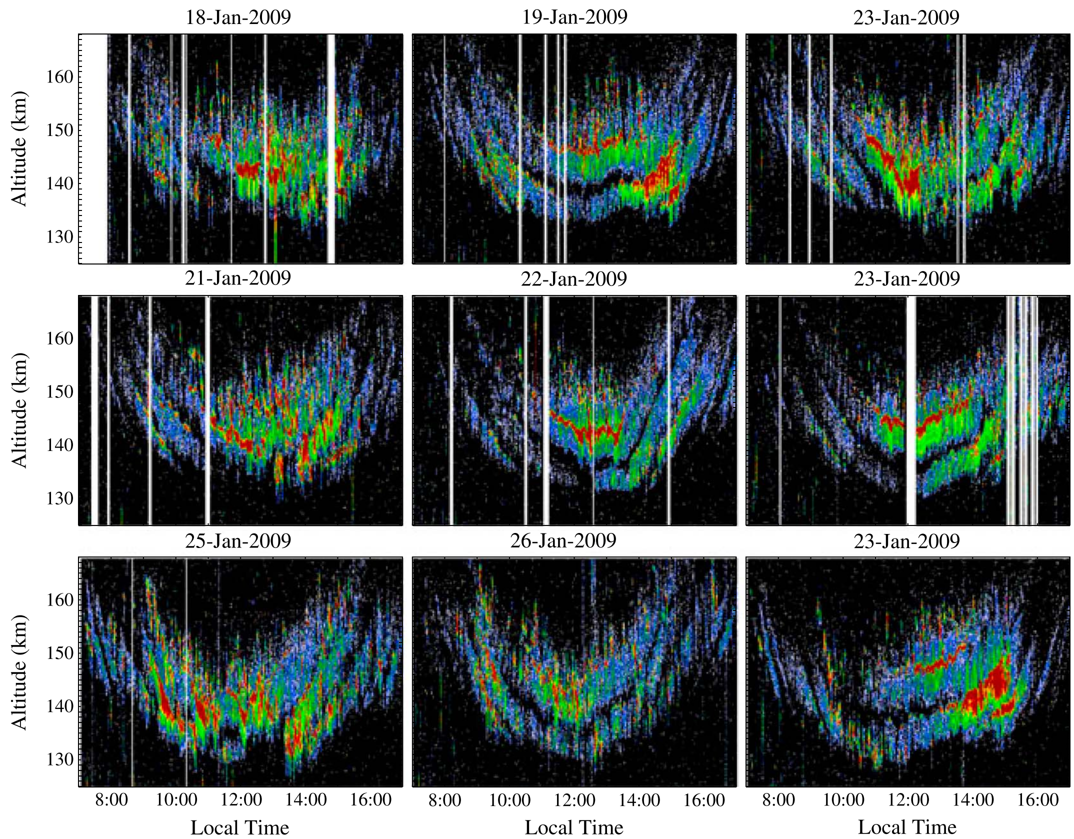

Figure 1. Example of 150 km radar echoes from the JRO 50 MHz radar. These are sometimes called "necklace echoes" because of their appearance in range-time-intensity plots like these [from *Chau and Kudeki*, 2013].

Observatory has detected enhanced electron plasma lines since the 1960s. These measurements were quickly associated with photoelectron excitation of Langmuir waves [*Carlson Jr.*, 1966; *Perkins et al.*, 1965]. More recently, high-resolution Arecibo measurements showed detailed spectra and revealed how plasma lines split when the plasma frequency approaches the second electron gyroharmonic [*Bhatt et al.*, 2008]. Other radars with sufficient sensitivity and receiver bandwidth measured similar electron line enhancements [*Nilsson et al.*, 1996; *Heinselman and Vickrey*, 1992].

Observations of 150 km echoes at JRO showed that these echoes appear with a variety of characteristics. *Chau* [2004] showed that the strongest 150 km echoes arrive from highly field-aligned structures and that these have the narrow spectral widths (<6 m/s). However, when examining echoes from a degree or two off of **B**, the spectral width expands greatly, to larger than the acoustic speed. *Chau and Kudeki* [2013] went on to show that the most common form has a spectral width that scales with power and a less common, but larger amplitude, type with a spectral width mostly independent of amplitude. In both cases, the spectral width does not exceed 6 m/s, making it one of the narrowest coherent echo signatures observed.

In the ionosphere at around 150 km altitude, energetic shell distributions of photoelectrons form during the daytime. Some of the clearest measurements were reported by *Lee et al.* [1980] using AE-E spacecraft data as seen in Figure 2. They show that between 22 and 27 eV, a series of local peaks arise from photoionization of N_2 and O_2 by solar He II (304 A) radiation. They also show a 5 eV peak in the spectrum that appears because, at 2.3 eV, a resonance in the electron N_2 scattering cross section causes a bite out in the distribution function leading to a distinct peak at 5 eV. This effect exists between 100 and 200 km altitude but has a maximum precisely where 150 km echoes maximize, between 135 and 155 km altitude [see *McMahon and Heroux*, 1983, Figure 6]. Similar observations were also reported by AE-C and rocket researchers [*Doering et al.*, 1970, 1975].

A number of theories have attempted to explain the origin of 150 km echoes. *Kudeki and Fawcett* [1993] proposed that a wind-driven gravity wave interchange instability underlies these waves and the periodicity in the vertical structure supports that idea. *Patra* [2011] argued that descending ion layers, possibly with a high

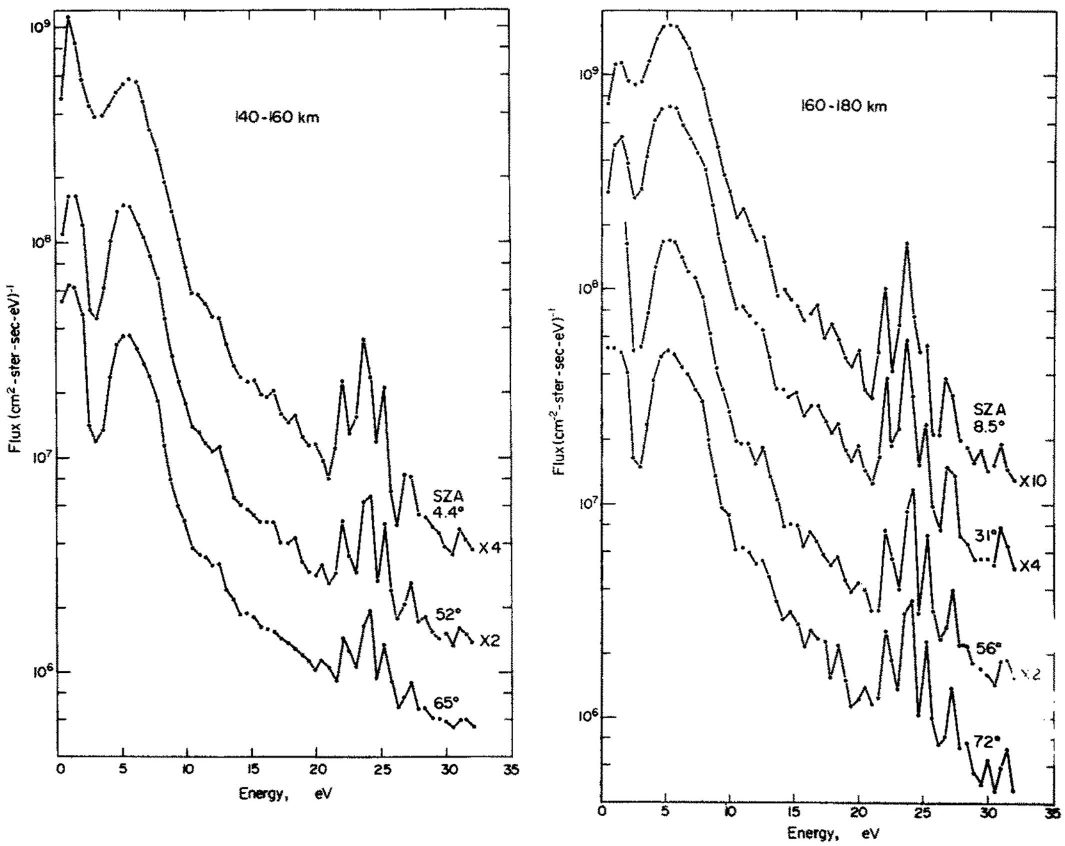

Figure 2. Measured photoelectron distributions from *Lee et al.* [1980].

concentration of metallic ions, could generate these gradients. However, the gradients and the winds do not appear consistently strong enough to account for the regularity of 150 km echoes. *Chau and Kudeki* [2013] write that "we still have no clear understanding of the processes responsible" for these waves.

The interactions of photoelectrons with a cold background plasma distribution have received some attention [*Forme*, 1999; *Diaz et al.*, 2010]. More generally, beam-plasma interactions parallel to a strong magnetic field have been studied for a half century, and the complex and diverse physics that results continues to receive attention. In the ionosphere, most of the attention has focused on bump-on-tail, two-stream, and ion-electron streaming instabilities resulting from precipitation and artificial electromagnetic heater-induced beams. In the ionosphere, research has focused on beam-plasma interactions perpendicular to the *B* field [*Basu et al.*, 1982].

2. Methods

This study used the kinetic 2-D and 3-D Electrostatic Parallel Particle-in-Cell (EPPIC) simulator as described in *Oppenheim and Dimant* [2013] with the addition of a population of photoelectrons. This simulates the dynamics of charged particles as they respond to internally generated electric fields with a constant background magnetic field. *Oppenheim et al.* [2008] describe many of the techniques applied by this simulator, and *Oppenheim and Dimant* [2004] discuss many of its limitations, though both of these focused on 2-D simulations. The simulations described in this paper were massively parallel but not extremely expensive, mostly using 1024 processors simultaneously. To reduce the expense of these simulations, they used an electron-to-ion mass ratio of 1024, making the simulation ions ~64 times lighter than in the ionosphere. The simulations presented in this work apply periodic boundary conditions. The remainder of this section will discuss aspects of these simulations unique to this problem and their limitations.

These runs initially position the particles uniformly throughout the simulation space and assign initial velocities to make the particle distribution Maxwellian. As a result of the discreteness of the particles, an initial nonzero noise level exists which substantially exceeds that found in nature and the waves grow from this

Table 1. Baseline Simulation Parameters With $\omega_e = 4 \times 10^7 \mathrm{s}^{-1}$ and $\lambda_D = 5 \times 10^{-3}$ m

Parameter	Normalized	Value
$L_{x,y}$	$1024\lambda_D$	5.12 m
# cells$_{x,y}$	1024	
Δt	$0.05\omega_e^{-1}$	1.25 ns
m_e	$m_i/1024$	4.9×10^{-29} kg
Ω_e	$0.577\omega_e$	23×10^6 s^{-1}
v_{s0}	$15v_{\mathrm{th}}$	11 eV
v_{sth}	v_{th}	0.05 eV
ν_e	$10^{-5}\omega_e$	400 s$^-$1
ν_i	$5 \times 10^{-5}\omega_e$	2000 s$^-$1
t_{end}	$15{,}800\omega_e$	0.4 ms

numerical noise. The total averaged electric field $\langle E^2 \rangle$ of the saturated state waves exceeds the initial noise by at least 1 order of magnitude.

The simulation mimics the photoelectron population by starting with a distribution of electrons having a high average velocity v_{s0} and the same thermal temperature as the background electrons but traveling in random directions, creating a shell in velocity space. In the atmosphere, solar EUV radiation creates this population of photoelectrons by ionizing neutral molecules and decelerates them via collisions and plasma-wave interactions. Ultimately, electrons recombine back into neutrals, but these generally come from the much larger cold thermal population. To create a quasi-equilibrium, the simulator takes electrons from the cold population and accelerates them to photoelectron velocities at a rate meant to mimic conditions at noon at the equator.

A broad range of simulation parameters were evaluated, but they are all variants of a baseline simulation. This simulation includes a cold core of electrons, an isotropic population of photoelectrons at a much higher energy, and a cold core of ions. Table 1 shows the parameters for the baseline simulation in dimensionless quantities and in physical units appropriate to 150 km at 14:00 local time near the magnetic equator at equinox.

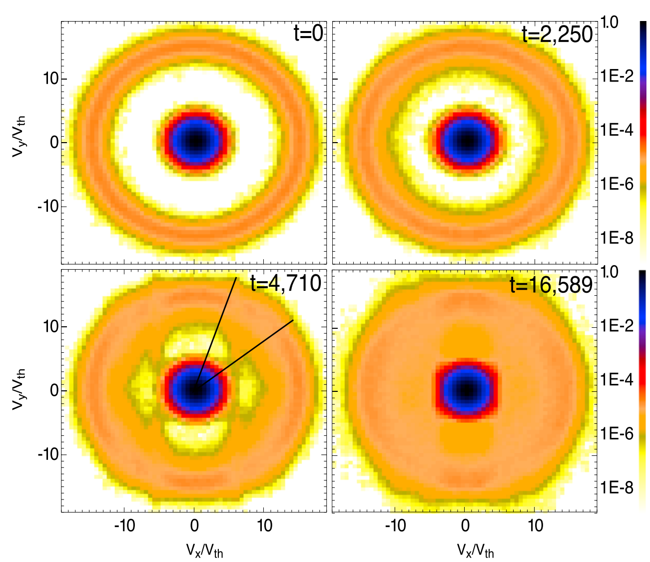

Figure 3. Velocity distribution evolution. The time shown has units of ω_e^{-1}. The bottom left ($t = 4710$) panel has two black lines indicating the pitch angles that decelerate most rapidly due to plasma-wave interactions. These create the vertical orange lines as they descend toward the x axis, showing that a population of electrons lose $v_\perp (= v_y)$ without losing $v_\parallel (= v_x)$. At the end of the simulation, a nearly steady state distribution function ($t = 16,589$) shows a loss of isotropy in the photoelectron shell population.

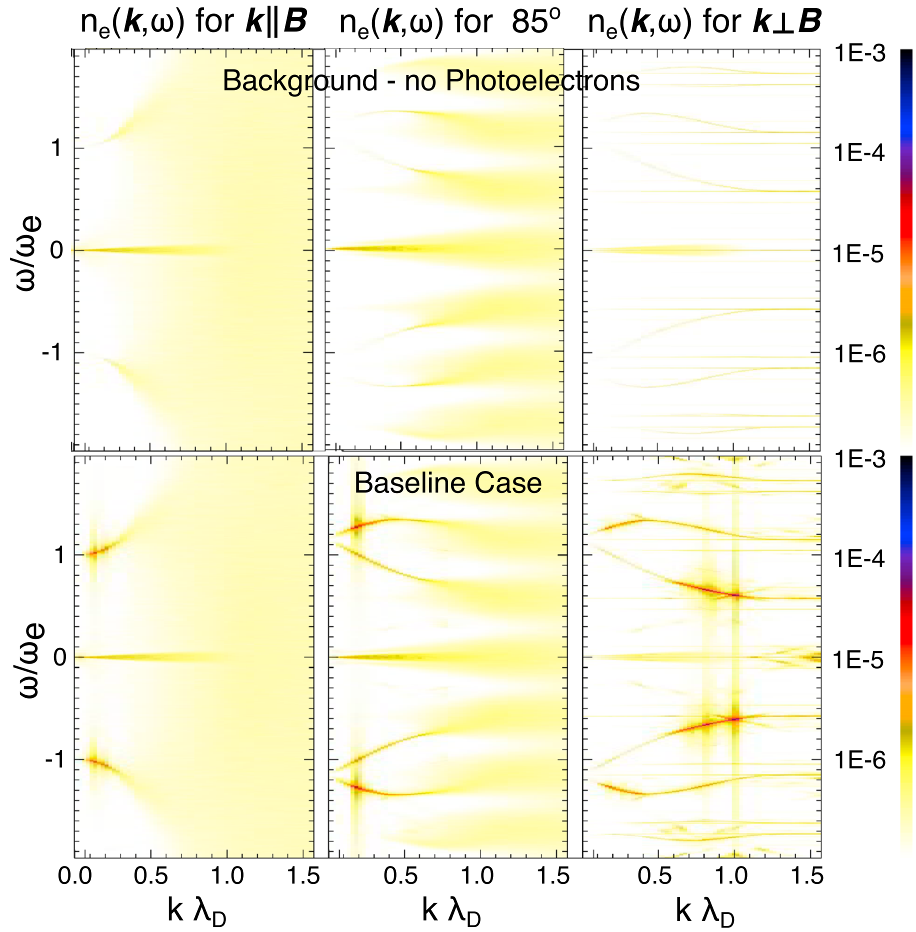

Figure 4. Electron density spectra at a range of angles with respect to $\vec{B}$. The frequency is normalized to the plasma frequency, ω_e, and the wave number is normalized to the Debye length, λ_D. Spectra showing (top row) the "noise case" and (bottom row) the baseline case.

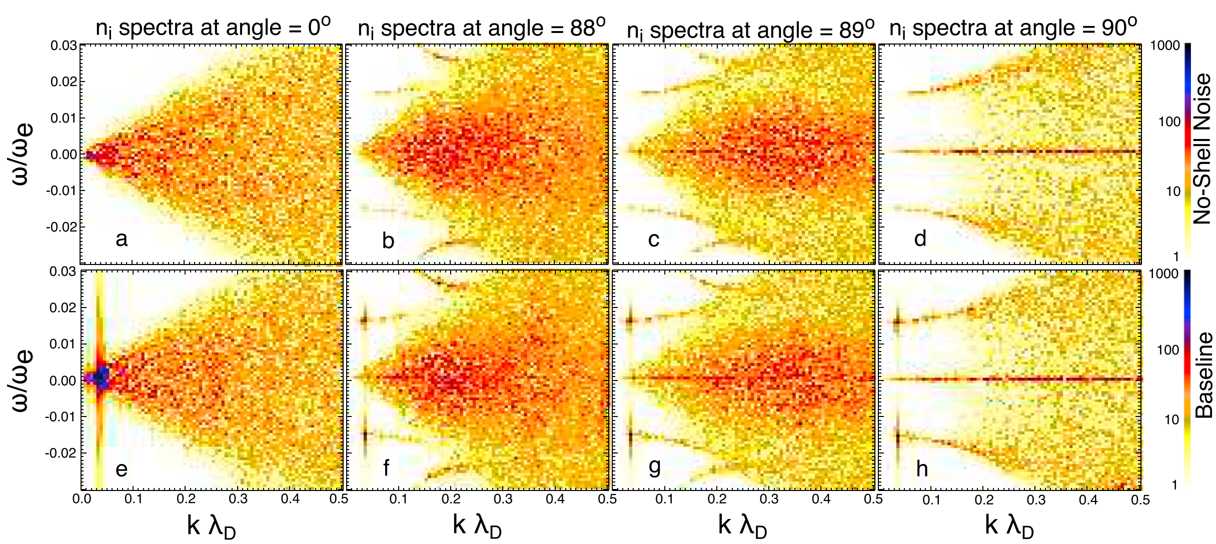

Figure 5. Ion density spectra at four angles from baseline and noise simulations. The angle is with respect to $\vec{B}$. Acoustic waves appear as the numerous modes bounded by the straight lines starting at $(k, \omega) = (0, 0)$ with slopes defined by the acoustic speed (a–c and e–g). Lower hybrid modes appear starting at roughly $(k\lambda_D, \omega/\omega_e) = (0.05, 0.0165)$ and proceeding to the right parabolically (b–d, f, and g). An unidentified higher-frequency mode appears in Figures 5b, 5c, 5f, and 5g starting at $\sim (k\lambda_D, \omega/\omega_e) = (0.14, 0.03)$. The spread in frequency seen in Figure 5e, at long wavelengths, arises because the simulation only completes a few oscillations (despite the >300,000 time steps) for these modes. A Fourier transform of a limited number of oscillations will add a breadth of frequency components.

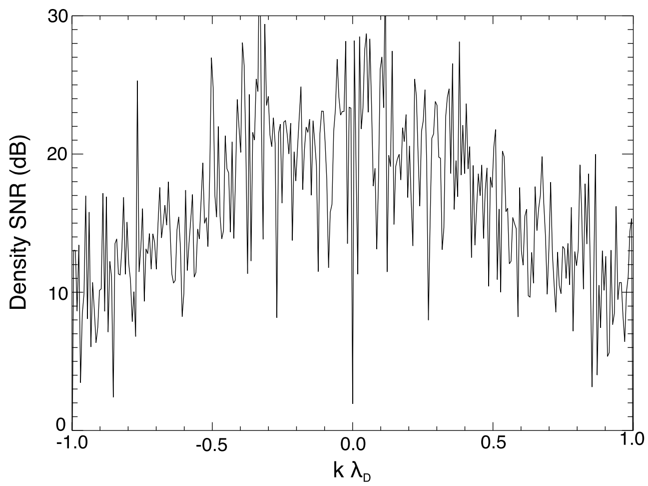

Figure 6. Ratio of power in dB of baseline case to noise case from $n_i(k_{x=0}, k_y, \omega = 0)$.

3. Results

The simulations show that the photoelectrons lose energy to electron plasma waves faster than they lose energy due to collisions with neutrals. The evolution of the electron distribution function from a cold thermal core plus a shell shows this clearly, as seen in Figure 3. By the end of the runs, these simulations reach a nearly steady state system where the shell electrons lose energy to waves and collisions at the same rate they are replenished by electrons boosted from the core distribution. These changes to the distribution function evolve over many thousands of plasma periods.

A close examination of this evolution shows an initial isotropic deceleration of the photoelectrons due to collisions. Then, a group of electrons with pitch angles between 36° and 69° (seen in the Figure 1, bottom left panel) begins to descend toward the $\hat{v}_x$ axis ($\hat{x} \parallel \vec{B}$). This breaks the symmetry and fills in phase space unevenly. This nonisotropic evolution appears more clearly in simulations with no collisions. This type of evolution exists in all the magnetized runs. In unmagnetized simulations, the shell fills in uniformly throughout phase space due to collisions. In simulations with no collisions and no $\vec{B}$, the shell fills in extremely slowly, probably due to collisions between particles and the turbulent fluctuation-dissipation electric fields.

The energy from the slowing photoelectrons goes into electron waves as seen in the spectra shown in Figure 4 and in animations of the electron density (see the supporting information). Figure 4 (bottom row) shows spectra from the baseline case, while Figure 4 (top row) shows the results for an identical run with no shell of photoelectrons, i.e., a “noise run.” Comparing the spectra for these two runs shows that energy goes both into plasma waves parallel to $\vec{B}$ and harmonics of the cyclotron frequency (electron Bernstein modes). These spectra should account for enhanced plasma lines as observed by radars.

The 150 km echoes result from reflections from enhanced wave-like irregularities in the plasma density. Even in an undisturbed warm plasma, large radars receive reflections from thermal fluctuations of ion-acoustic waves, allowing measurements of plasma density and temperature via “incoherent scatter.” To explain 150 km echoes, one needs a 10–20 dB enhancement of low-frequency waves above the background thermal fluctuations at the radar wavelength. Figure 5 shows that these simulations predict just such an enhancement driven by the electron waves.

Figure 5 (top row) presents spectra from the noise simulation for four different angles, showing the incoherent scatter spectra for a range of $\vec{k}$ values. Figure 5 (bottom row) displays the same spectra for the baseline run, showing an enhanced set of small-k ion-acoustic modes at small aspect angles. As one goes to higher aspect angles, one sees only small increases in ion-acoustic mode energy and an enhancement at the long-wavelength, higher-frequency ($\omega/\omega_e \approx 0.016$) lower hybrid modes. At an aspect angle of 90°, one sees essentially no acoustic wave energy but instead energy at small $\omega \sim 0$ for all k. At 89°, both an enhancement at $\omega \sim 0$ and a small amount of acoustic energy appear. If one picks a specific wavelength such as 3 m, the simulation produces a spectrum that reproduces the measurements in *Chau* [2004] (Figure 2).

The spectra at 90° are distinct from that at all other angles. Examining spectra at a range of angles from 89.5° to 90° (not shown) shows the acoustic mode narrowing in frequency range toward $\omega = 0$ as the angle approaches 90°. Also, the enhancement of energy in the small-ω modes for the baseline case over the noise case becomes more apparent. Figure 6 shows the ratio of the power from the noise run to the baseline case such that $\mathrm{SNR} = 10\log_{10}[\tilde{n_{ib}}(k_x = 0, k_y, \omega = 0)/\tilde{n}_{in}(k_x = 0, k_y, \omega = 0)]$ where $\tilde{n_{ib}}$ and $\tilde{n_{in}}$ are the amplitudes of the Fourier transformed densities from the baseline and noise runs, respectively. This shows a clear enhancement that may explain the 50 MHz JRO radar measurements near 150 km [*Chau et al.*, 2009].

4. Discussion and Conclusions

These simulations show both enhanced electron and ion waves resulting from energetic photoelectrons interacting with a cold background plasma subject to the geomagnetic field. Large radars with bandwidth sufficient to detect electron lines such as Arecibo measure just such enhanced waves as plasma lines, and equatorial radars observe enhanced ion lines around 150 km. Simulations of this type can demonstrate how these lines change as a function of angle with respect to $\vec{B}$, plasma density, temperature, composition, and energetic particle distribution.

The enhanced ion modes reproduce many features of 150 km echoes. Figure 6 shows enhanced ion lines perpendicular to $\vec{B}$ ($\omega \approx 0$) with an amplitude many times the noise level, similar to that observed by *Chau et al.* [2009]. Figure 5 shows that perpendicular modes ($\theta = 90$) have narrow spectra (in ω). The current simulator may be able to compare the width of these spectral lines with their power as done in *Chau and Kudeki* [2013], but that will require an extensive set of longer runs. These simulations also reproduce the *Chau* [2004] (Figure 2) radar measurement showing echoes a degree or two away from $\vec{B}$ having both a high-amplitude peak at $\omega = 0$ with a narrow spectral width and a weaker amplitude having a spectral width near the acoustic speed.

The simulations also predict that a variety of enhanced modes will exist at the same time as 150 km echoes. Figure 4 shows a range of enhanced electron modes from Langmuir to cyclotron (Bernstein) and upper hybrid waves. It also develops enhanced lower hybrid modes for a select range of wavelengths. Ideally, a radar or set of radars could look for these coincident with 150 km echoes.

A series of comparison runs for a range of different ring energies and plasma densities was performed, but extensive discussions of these require a longer, more complete study. Also, a large and expensive 3-D run was performed but showed only minor differences from the 2-D ones presented here.

The wave-particle interactions that create the enhanced electron modes have been explored theoretically. These may be instability processes as discussed in *Nilsson et al.* [1996], *Perkins et al.* [1965], and *Jasperse et al.* [1995]. Modes parallel to $\vec{B}$ can result from bump-on-tail-type instabilities, while those perpendicular to $\vec{B}$ can derive from kinetic instabilities in magnetized plasmas as discussed in *Basu et al.* [1982]. However, neither of these will perfectly capture the evolution as simulated since most of the energy comes from photoelectrons that have pitch angles near 45°, and these particles primarily lose their perpendicular energy. The wave enhancements due to the photoelectrons may not result from a linear instability but from fluctuation enhancement that occurs as a plasma approaches instability [*Sitenko*, 1982]. This needs a more thorough analysis.

The simulation with photoelectrons shows strong enhancements of electron cyclotron and upper hybrid modes above the noise-only run. *Jasperse et al.* [1995] showed that cyclotron waves should preferentially occur when $\omega_{\mathrm{UH}} = n\Omega_e$ where ω_{UH} is the upper hybrid frequency, Ω_e is the electron cyclotron frequency, and n is an integer, $n \geq 2$. The baseline simulation explores the $n = 2$ condition, showing a dramatic increase in cyclotron mode energy compared to a nonresonant simulation where $n = 2.5$. However, an $n = 3$ resonant simulation does not show a dramatic enhancement of these modes above the $n = 2.5$ one. This type of simulation gives us a new tool to explore photoelectron-generated electron turbulence, and we plan to engage in a more detailed investigation in the near future.

The nature of the wave-wave interactions leading to the enhancement of the ion lines remains poorly understood although research related to auroral precipitation may provide some insights [*Forme*, 1999; *Diaz et al.*, 2010]. The simulator provides us with a tool to enable us to better understand this mechanism and resulting observational characteristics.

Reyes [2012] showed the evolution of 150 km echoes during a solar flare event. While our model helps one understand the strong enhancement of the echoes, it does not yet help us understand the detailed structure of the enhancement as they rapidly change altitude. This model suggests extensive continued research. One could confirm (or debunk) this model by comparing solar EUV emission strength with 150 km echo amplitudes.

Both 150 km echoes and plasma line measurements show a broad array of characteristics that this model may explain. For instance, the vertical structure of 150 km echoes may appear because of specific resonances. *Kudeki and Fawcett* [1993] have suggested that density gradients may play an essential role or there may be resonances along $\vec{B}$ where the length of the field line before it encounters the lower conductivity D region causes the field lines to vibrate like "guitar strings." We have not tested these ideas, but they may modulate the driver put forward here. More extensive simulations and analysis should allow us to understand the underlying mechanisms of these measurements.

Acknowledgments
The authors would like to thank Juha Vierinen, David Hysell, Jorge Chau, and Roger Varney for their helpful discussions and suggestions. This material is based upon work supported by NASA under grant NNX14AI13G. This work used the XSEDE and TACC computational facilities, supported by National Science Foundation grant ACI-1053575. Simulation-produced data are archived at TACC and available upon request.

References

Balsley, B. B. (1964), Evidence of a stratified echoing region at 150 kilometers in the vicinity of the magnetic equator during daylight hours, *J. Geophys. Res.*, *69*, 1925–1930.

Basu, B., T. Chang, and J. R. Jasperse (1982), Electrostatic plasma instabilities in the daytime lower ionosphere, *Geophys. Res. Lett.*, *9*, 68–71, doi:10.1029/GL009i001p00068.

Bhatt, A. N., M. J. Nicolls, M. P. Sulzer, and M. C. Kelley (2008), Observations of plasma line splitting in the ionospheric incoherent scatter spectrum, *Phys. Rev. Lett.*, *100*, 045005, doi:10.1103/PhysRevLett.100.045005.

Carlson, H. C., Jr. (1966), Ionospheric heating by magnetic conjugate-point photoelectrons, *J. Geophys. Res.*, *71*, 195–199, doi:10.1029/JZ071i001p00195.

Chau, J. L. (2004), Unexpected spectral characteristics of VHF radar signals from 150-km region over Jicamarca, *Geophys. Res. Lett.*, *31*, L23803, doi:10.1029/2004GL021620.

Chau, J. L., and E. Kudeki (2013), Discovery of two distinct types of equatorial 150 km radar echoes, *Geophys. Res. Lett.*, *40*, 4509–4514, doi:10.1002/grl.50893.

Chau, J. L., R. F. Woodman, M. A. Milla, and E. Kudeki (2009), Naturally enhanced ion-line spectra around the equatorial 150-km region, *Ann. Geophys.*, *27*, 933–942.

Diaz, M. A., J. L. Semeter, M. Oppenheim, and M. Zettergren (2010), Analysis of beam plasma instability effects on incoherent scatter spectra, *Ann. Geophys.*, *28*, 2169–2175, doi:10.5194/angeo-28-2169-2010.

Doering, J. P., W. G. Fastie, and P. D. Feldman (1970), Photoelectron excitation of N_2 in the day airglow, *J. Geophys. Res.*, *75*, 4787–4802, doi:10.1029/JA075i025p04787.

Doering, J. P., W. K. Peterson, C. O. Bostrom, and J. C. Armstrong (1975), Measurement of low-energy electrons in the day airglow and day side auroral zone from Atmosphere Explorer C, *J. Geophys. Res.*, *80*, 3934–3944, doi:10.1029/JA080i028p03934.

Forme, F. R. E. (1999), Parametric decay of beam-driven Langmuir wave and enhanced ion-acoustic fluctuations in the ionosphere: A weak turbulence approach, *Ann. Geophys.*, *17*, 1172–1181, doi:10.1007/s00585-999-1172-4.

Heinselman, C. J., and J. F. Vickrey (1992), On the frequency of Langmuir waves in the ionosphere, *J. Geophys. Res.*, *97*, 14,905–14,910, doi:10.1029/92JA01143.

Jasperse, J. R., B. Basu, J. M. Retterer, D. T. Decker, and T. Chang (1995), High frequency electrostatic plasma instabilities and turbulence layers in the lower ionosphere, in *Space Plasmas: Coupling Between Small and Medium Scale Processes*, vol. 86, edited by M. Ashour-Abdalla, T. Chang, and P. Dusenbery, pp. 77, AGU, Washington, D. C.

Kudeki, E., and C. D. Fawcett (1993), High resolution observations of 150 km echoes at Jicamarca, *Geophys. Res. Lett.*, *20*, 1987–1990.

Lee, J. S., J. P. Doering, T. A. Potemra, and L. H. Brace (1980), Measurements of the ambient photoelectron spectrum from Atmosphere Explorer: I. AE-E measurements below 300 km during solar minimum conditions. II. AE-E measurements from 300 to 1000 km during solar minimum conditions, *Planet. Space Sci.*, *28*, 947–971, doi:10.1016/0032-0633(80)90058-6.

McMahon, W. J., and L. J. Heroux (1983), The 2- to 5-eV energy spectra of thermospheric photoelectrons: Measurements in apparent conflict with theory, *J. Geophys. Res.*, *88*, 9249–9254, doi:10.1029/JA088iA11p09249.

Nilsson, H., S. Kirkwood, J. Lilensten, and M. Galand (1996), Enhanced incoherent scatter plasma lines, *Ann. Geophys.*, *14*, 1462–1472, doi:10.1007/s00585-996-1462-z.

Oppenheim, M. M., and Y. S. Dimant (2004), Ion thermal effects on E-region instabilities: 2-D kinetic simulations, *J. Atmos. Solar Terr. Phys.*, *66*, 1639–1654.

Oppenheim, M. M., and Y. S. Dimant, (2013) Kinetic simulations of 3-D Farley-Buneman turbulence and anomalous electron heating, *J. Geophys. Res. Space Physics*, 1306–1318, doi:10.1002/jgra.50196.

Oppenheim, M. M., Y. Dimant, and L. P. Dyrud (2008), Large-scale simulations of 2-D fully kinetic Farley-Buneman turbulence, *Ann. Geophys.*, *26*, 543–553.

Patra, A. K. (2011), Descending ion layer property in the Gadanki radar observations of 150 km echoes and its implication to the echoing phenomenon, *J. Geophys. Res.*, *116*, A11322, doi:10.1029/2011JA016805.

Patra, A. K., P. Pavan Chaitanya, and D. Tiwari (2011), Characteristics of 150 km echoes linked with solar eclipse and their implications to the echoing phenomenon, *J. Geophys. Res*, *116*, A05319, doi:10.1029/2010JA016258.

Perkins, F. W., E. E. Salpeter, and K. O. Yngvesson (1965), Incoherent scatter from plasma oscillations in the ionosphere, *Phys. Rev. Lett.*, *14*, 579–581, doi:10.1103/PhysRevLett.14.579.

Reyes, P. M. (2012), Solar flare effects observed over Jicamarca during MST-ISR experiments, Master's thesis, Univ. of Illinois, Urbana-Champaign.

Rodrigues, F. S., E. B. Shume, E. R. de Paula, and M. Milla (2013), Equatorial 150 km echoes and daytime F region vertical plasma drifts in the Brazilian longitude sector, *Ann. Geophys.*, *31*, 1867–1876, doi:10.5194/angeo-31-1867-2013.

Sitenko, A. G. (1982), *Fluctuations and Non-Linear Wave Interactions in Plasmas,* chap. 6, Pergamon Press, New York.

Yokoyama, T., D. L. Hysell, A. K. Patra, Y. Otsuka, and M. Yamamoto (2009), Zonal asymmetry of daytime 150-km echoes observed by Equatorial Atmosphere Radar in Indonesia, *Ann. Geophys.*, *27*, 967–974.